Nanoscale

PAPER

View Article Online
View Journal | View Issue

Cite this: *Nanoscale*, 2020, **12**, 13501

Origin of ferromagnetism and the effect of doping on Fe_3GeTe_2†

Seung Woo Jang,[a] Hongkee Yoon,[a] Min Yong Jeong,[a] Siheon Ryee,[a] Heung-Sik Kim[b] and Myung Joon Han *[a]

Received 1st December 2019,
Accepted 18th May 2020

DOI: 10.1039/c9nr10171c

rsc.li/nanoscale

Recent experimental findings of two dimensional ferromagnetism in Fe_3GeTe_2, whose critical temperature can reach room temperature by gating, has attracted great research interest. Here we performed elaborate *ab initio* studies using density functional theory, dynamical mean-field theory and magnetic force response theory. In contrast to the conventional wisdom, it is unambiguously shown that Fe_3GeTe_2 is not ferromagnetic but is antiferromagnetic, carrying zero net moment in its stoichiometric phase. Fe defect and hole doping are the keys to make this material ferromagnetic as supported by previously disregarded experiments. Furthermore, we found that electron doping also induces the antiferro- to ferro-magnetic transition. It is crucial to understand the notable recent experiments on gate-controlled ferromagnetism. Our results not only reveal the origin of ferromagnetism of this material but also show how it can be manipulated with defects and doping.

1 Introduction

Recently, magnetic 2-dimensional (2D) van der Waals (vdW) materials have attracted tremendous attention.[1–28] On the one hand, magnetic ordering in 2D limit is in itself an interesting physical phenomenon.[29] On the other hand, from the point of view of device applications, they have great potential for the electrical control of magnetism and spintronic devices.[1,2,13–18,28] Based on ferromagnetic (FM) materials, in particular, recent experiments have shown many fascinating phenomena and useful possibilities such as electronically tunable magnetism,[16,23] room-temperature ferromagnetism,[8,23] and controlled spin and valley pseudospins.[11]

In this regard, great research efforts are now being devoted to Fe_3GeTe_3 (FGT). Bulk FGT is known as a FM metal with a critical temperature of T_c, 220 K.[30–33] Its 2D form has recently been reported by Fei *et al.* who showed that the ferromagnetism of this material survives down to the mono-layer.[10] Furthermore, Deng *et al.* demonstrated that its T_c can be controlled by gating, and can eventually reach room temperature.[23] It is certainly a useful feature for device applications. Other intriguing and promising aspects of FGT include its applicability to the tunneling spin valve,[3] patterning-induced ferromagnetism,[25] thickness-dependent hard magnetic phase,[27] large anomalous Hall current driven by topological nodal lines,[26] and Kondo behavior.[22]

In this study, we start with a motivation that the origin of ferromagnetism of FGT is still not clearly understood.[34] First of all, we show that the magnetic ground state of stoichiometric FGT is not FM, which is in sharp contrast to various experimental reports but is consistent with the recent total energy result.[34] Our extensive calculations of total energies and magnetic force responses establish that the inter-layer coupling in FGT is antiferromagnetic (AFM). Second, it is the defects that make this material FM. It is found that introducing a small amount of Fe defects or hole doping causes the inter-layer coupling to quickly become FM. This conclusion is consistent with the previous experimental reports about the difficulty in synthesizing stoichiometric samples without Fe deficiency. Finally, we demonstrate that a FM order can also be induced by electron doping. It is of crucial importance to understand the recent experiment by Deng *et al.*[23] Our current work sheds new light on understanding the origin of ferromagnetism in FGT and how to manipulate it through defect and doping.

2 Results and discussion

2.1 AFM ground state

Fig. 1(a) presents the calculated total energy difference between the inter-layer (out-of-plane) AFM and FM spin order in bulk FGT; $\Delta E = E_{AFM} - E_{FM}$ (within the plane, the FM order

[a]*Department of Physics, Korea Advanced Institute of Science and Technology (KAIST), Daejeon 34141, Republic of Korea. E-mail: mj.han@kaist.ac.kr*
[b]*Department of Physics, Kangwon National University, Chuncheon-Si, Gangwon-Do, 24341, Republic of Korea*

†Electronic supplementary information (ESI) available. See DOI: 10.1039/C9NR10171C

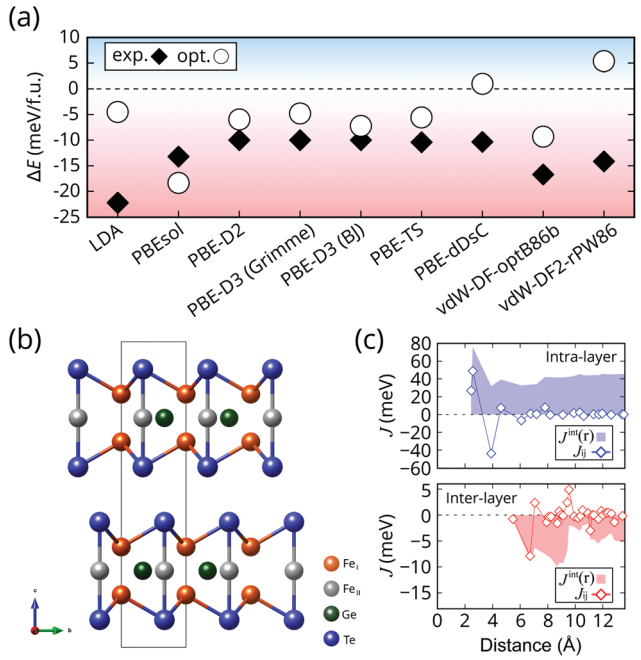

Fig. 1 The magnetic interaction and the ground state of undoped bulk FGT. (a) The calculated total energy differences (ΔE) between AFM and FM inter-layer order using various XC-vdW functionals. The results from the experimental[30] and the optimized structures are indicated by diamonds (black) and circles (white), respectively. (b) The side view of the FGT structure. Fe_I, Fe_{II}, Ge, and Te atoms are represented by orange, gray, green, and blue spheres, respectively. Fe_I and Fe_{II} represent two inequivalent Fe sites with +3 and +2 formal charge states, respectively. (c) The calculated magnetic couplings, J_{ij}, as a function of inter-atomic pair distance (also taking the coordination number into account; *i.e.*, all equal distance interactions represented by one symbol). The intra- and inter-layer interactions are represented in the upper and lower panel, respectively. The filled curves (shaded areas) show the integrated values of J_{ij} up to the given distance; $J^{int}(r) = \sum_0 J_{ij}$.

is always favored; not shown). We pay special attention to the fact that describing the vdW interaction within the density functional theory (DFT) framework needs care because the exchange–correlation (XC) functional form for this weak interaction has not yet been quite well established.[35–40] As a practical way to resolve this issue and to investigate the ground state spin order, we adopted 9 different functional forms.[35–48] We also considered both the experimental (black diamonds) and the optimized structures (white circles). It is clearly seen that the AFM inter-layer coupling is energetically more stable in most of the functionals. The only exception is the fully-relaxed structure with the so-called 'vdW-DF2-rPW86' functional.[48] This functional, however, significantly overestimates the lattice parameters (see the ESI, Section 1† for more details). In the case of the 'PBE-dDsC' functional,[46,47] the FM order is slightly more favorable, but its energy difference from AFM is too small (~0.98 meV per f.u.). We also performed the self-consistent DFT + dynamical mean field theory (DMFT) calculations to take the dynamic on-site electron correlation within Fe-3d orbitals into account. The result also supports the AFM ground state; $\Delta E = E_{AFM} - E_{FM} \simeq -22$ and -14 meV per f.u. from the two different so-called 'double-counting' functional choices. Note that the DMFT energy difference is substantially larger than that calculated by DFT. We hereby conclude that the inter-layer magnetic configuration of FGT is AFM.

In order to nail down this conclusion, namely, the AFM inter-layer coupling, we performed magnetic force theory (MFT) calculation which measures the magnetic moment response at one atomic site to the perturbative change at another.[49–52] The results are summarized in Fig. 1(c); the intra-layer (within the plane) and inter-layer magnetic couplings are shown in the upper and lower panel, respectively. Since our MFT calculation is conducted in the momentum space and then transformed into the real space,[52] all inter-atomic pair interactions are obtained in a single response computation. In Fig. 1(c), we present them as a function of inter-atomic distance where the coordination number has been taken into account (namely, the calculated J_{ij} is multiplied by the coordination number so that each data point represents the magnetic interaction strength at a given distance; for a different plot, see the ESI, Section 2†). As the inter-atomic distance becomes larger, J_{ij} is reduced and eventually becomes zero as expected. The first thing to be noted is the FM intra-layer coupling. The integrated magnetic interaction $J^{int}(r)$ (*i.e.*, the sum of all pair interactions J_{ij} up to the given distance r; represented by the colored area) clearly shows that the intra-layer magnetic interaction is always FM, and it is dominated by the first two FM couplings.

Importantly, the inter-layer magnetic interaction is AFM. The lower panel of Fig. 1(c) shows that, although there are many FM inter-atomic pair interactions along the out-of-plane direction, the overall interaction is steadily AFM; $J^{int}(r)$ remains negative (the shaded area). The second neighboring AFM pair dominates the inter-layer interaction and stabilizes the AFM order. We emphasize that both total energy and magnetic force calculation unequivocally indicate that stoichiometric FGT is AFM carrying zero net moment.

2.2 Fe defect, hole-doping and the FM ground state

Seemingly, this conclusion is in sharp contrast to the results of various experiments because FGT is known as a FM metal for both bulk and thin film. Here we identify, however, that the crucial factor to stabilize ferromagnetism is hole doping. According to the literature, it seems quite difficult to make defect-free stoichiometric FGT, and the sample easily becomes Fe-deficient.[30,32,33,53–55] Since Fe deficiency induces hole doping, we investigate its effect on the magnetic order which has never been studied before.

First, we calculated the total energy difference ΔE as a function of doping. Fig. 2(a) clearly shows that introducing ~0.2–0.6 holes per formula unit (f.u.) induces the AFM to FM transition.

This level of hole doping is in good agreement with the Fe defect concentration reported in experiments:[56] $0.11 < x < 0.36$ for single crystalline $Fe_{3-x}GeTe_2$ or powder,[30,32,33,53–55] and $0.03 < x < 0.31$ for a polycrystalline sample[33] although its

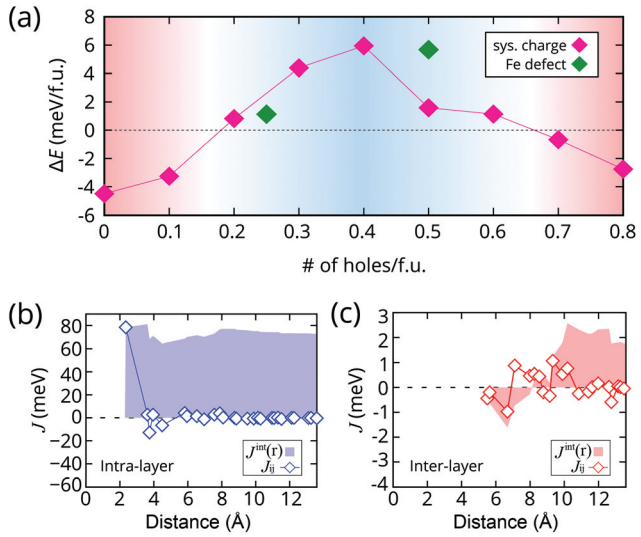

Fig. 2 The magnetic interaction and the ground state of hole-doped bulk FGT. (a) The calculated total energy differences (ΔE) between the inter-layer AFM and FM phases as a function of hole concentration. The magenta and green symbols are the results of the calculation with varying system charge and the supercell calculation with Fe defects, respectively. For the latter, the doping concentration is determined by assigning three and two holes for one deficient Fe_I and Fe_{II}, respectively. (b and c) The calculated intra-layer (b) and inter-layer (c) magnetic couplings obtained from the supercell calculation of $Fe_{2.75}GeTe_2$ (0.5 hole doping per f.u.). The calculated J_{ij} and $J^{int}(r)$ are represented with diamond symbols and the filled curves (shaded areas), respectively.

relationship to the magnetic ground state has never been discussed nor speculated.[57]

We think that a similar amount of Fe defects can likely be present in the thin-film samples as well (no refinement data reported yet).

Second, we perform the supercell total energy calculation to directly simulate the Fe-deficient sample. In our supercell setups, $Fe_{2.75}GeTe_2$ and $Fe_{2.875}GeTe_2$ can be simulated, and the simulation results are in good agreement with the experiments.[30,32,33,53–55] The results are shown as green diamond symbols in Fig. 2(a). This clearly shows that, with Fe defects, the FM order is energetically favorable, $\Delta E > 0$.

Finally, we perform the MFT calculation to double check this conclusion. The results of $Fe_{2.75}GeTe_2$ are summarized in Fig. 2(b) and (c) which present the intra- and inter-layer interactions, respectively. Note that the inter-layer interaction changes to become FM (*i.e.*, the shaded area of J_{int} becomes positive in Fig. 2(c)) while the intra-layer coupling remains FM (see Fig. 2(b)). For more detailed analysis, see the ESI, Section 3 and 4† which also provide discussion on the electronic structure change. Once again, this is a strong and independent confirmation that, upon hole doping, the inter-layer magnetic order is changed to FM. For further evidence that the defect and hole doping critically affect the magnetic properties of FGT, see the ESI, Section 5 and 6.† The latter, in particular, shows that the calculated magnetic moment with hole doping is in good agreement with the experimental values.

2.3 Electron doping and the recent gating experiment

Once we establish that stoichiometric FGT is AFM and that the FM order is induced by Fe defects or hole doping, an important new question arises. Recently, Deng *et al.* reported the gate tunability of ferromagnetism in ultra-thin FGT.[23] It has been demonstrated that the magnetic properties including T_c can be enhanced and manipulated by ionic gating. Here we note that their gating dopes electrons, not holes.

In order to understand the experiment and to answer this fundamentally important question, we investigate the effect of electron doping on the magnetic order. Remarkably, we found that electron doping also induces a FM order. To simulate the experimental conditions,[23] a Li atom is placed in the vicinity of the top surface of the FGT bi-layer; see the inset of Fig. 3. Due to the high electropositivity of Li, electrons are transferred and doped onto FGT. Fig. 3 presents the calculated ΔE as a function of the inverse height of the Li atom, $1/z_{Li}$ (z_{Li} is defined as the distance between Li and the top surface of FGT). $1/z_{Li}$ was reported to well represent the amount of doped electrons[58,59] (for more details, see the ESI, Section 7†). Note that the AFM to FM transition is induced by electron doping: in the high doping regime ($0.5 \leq 1/z_{Li} \leq 1$), the calculated ΔE is positive. As the height increases (*i.e.*, $1/z_{Li} \rightarrow 0$), FGT eventually becomes AFM as expected, corresponding to undoped FGT. This result elucidates the relationship between the electron doping and ferromagnetism of FGT, thereby establishing the physical picture for the recent experiment by Deng *et al.*[23]

2.4. Discussion

Our result can possibly provide further information to understand the gating experiment in more detail. An intriguing feature observed in ref. 23 is that the measured T_c and the coercive field exhibit a clear drop at around 1.4 volts before the rapid rise at around 1.8 volts which indicates that ferromagnetism is first suppressed and then revived as a function of electron doping. It might be interesting to think about the possibility that this behavior is at least partly related to the interplay between the Fe defects (or holes) and the doped electrons.

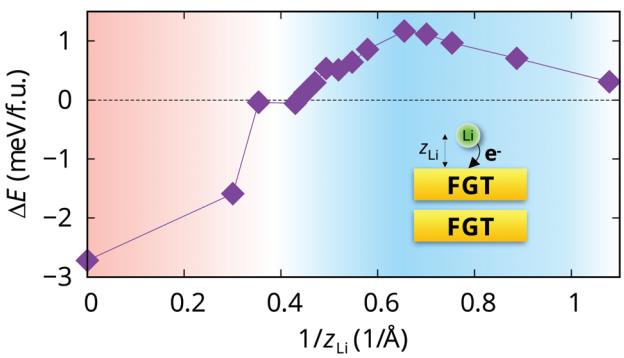

Fig. 3 The calculated ΔE as a function of the inverse height ($1/z_{Li}$) of Li atom. $1/z_{Li}$ is proportional to the amount of doped electrons in the FGT layers. The inset shows the schematic illustration of the electron doping from Li onto the FGT bi-layer.

Also, from the fact that the defect-free FGT is antiferromagnetically ordered along the out-of-plane direction, one can expect to realize the CrI_3-type magnetic geometry for this metallic material, which was suggested to be useful for device applications.[7,12–15,17,18]

3 Conclusions

To summarize, we, for the first time, identify the origin of ferromagnetism in FGT. Our total energy and MFT calculation unambiguously show that the defect-free stoichiometric FGT is AFM while introducing Fe defects or holes stabilizes the FM solution. Furthermore, it is demonstrated that electron doping induces the AFM to FM transition as well. It is crucially important to understand the recent gate control experiment in which the ionic gating dopes the thin film FGT with electrons.

4 Computational methods

We performed total energy and electronic structure calculations employing DFT as implemented in the VASP (Vienna *Ab initio* Software Package).[60] The local density approximation (LDA) XC functional[41] as parameterized by Perdew and Zunger[42] was used unless specified otherwise. To confirm the robustness of our conclusion, we double checked the undoped case with many different XC functionals and vdW corrections including PBE,[43] PBEsol,[44] D2,[35] D3 (Grimme),[36,39] D3 (BJ),[36,39] TS,[45] dDsC,[46,47] vdWDF-optB66b,[37,38,40] and vdW-DF2-rPW86.[48] For bulk FGT, a 700 eV energy cutoff and 18×4 k mesh in the first Brillouin zone were used. It is important to use a large enough k point grid (for related discussion, see the ESI, Section 8†). The force criterion for structure optimization was 5 meV $Å^{-1}$. The atomic positions are optimized for each case of AFM and FM structures. For simulating hole doping, we performed both calculations with varying system charges and the explicit Fe defects. For the latter, two different supercells were considered, corresponding to four- and eight-times f.u. with a single Fe vacancy. The defect is created at the Fe_{II} site, as known from the experiment.[33] For more details, see the ESI, Section 9† which also includes the defect formation energy calculation. In order to simulate the gating experiment of electron doping,[23] we performed the slab calculations with a Li atom on top of the FGT bi-layer. For bi-layer structures, the vacuum distance of ~25 Å was used with 600 eV energy cutoff and $14 \times 14 \times 1$ k points. The amount of electron doping was controlled by adjusting the Li-atom positions. For MFT calculations,[49–52] we used our DFT code, OpenMX.[61,62] Our DFT + DMFT calculations were performed using the DFT + embedded DMFT package based on Wien2K.[63] 'Nominal double-counting' scheme was adopted with two choices of $n_{Fe_I} = n_{Fe_{II}} = 6$ [53] and $n_{Fe_I} = 5$, $n_{Fe_{II}} = 6$.[23] Other computation details are basically the same as those of Zhu *et al.*[53] in which only ferromagnetic solution was calculated.

Conflicts of interest

There are no conflicts to declare.

Acknowledgements

We are grateful to H.-J. Sung, K. J. Chang and J. Im for useful discussion on the defect formation energy calculation. This work was supported by the Basic Science Research Program through the National Research Foundation of Korea (NRF) funded by the Ministry of Education (2018R1A2B2005204) and the Creative Materials Discovery Program through the NRF funded by the Ministry of Science and ICT (2018M3D1A1058754).

References

1 K. S. Burch, D. Mandrus and J.-G. Park, *Nature*, 2018, **563**, 47.
2 C. Gong and X. Zhang, *Science*, 2019, **363**, eaav4450.
3 X. Wang, K. Du, Y. Y. F. Liu, P. Hu, J. Zhang, Q. Zhang, M. H. S. Owen, X. Lu, C. K. Gan, P. Sengupta, C. Kloc and Q. Xiong, *2D Mater.*, 2016, **3**, 031009.
4 Y. Tian, M. J. Gray, H. Ji, R. J. Cava and K. S. Burch, *2D Mater.*, 2016, **3**, 025035.
5 J.-U. Lee, S. Lee, J. H. Ryoo, S. Kang, T. Y. Kim, P. Kim, C.-H. Park, J.-G. Park and H. Cheong, *Nano Lett.*, 2016, **16**, 7433–7438.
6 C. Gong, L. Li, Z. Li, H. Ji, A. Stern, Y. Xia, T. Cao, W. Bao, C. Wang, Y. Wang, Z. Q. Qiu, R. J. Cava, S. G. Louie, J. Xia and X. Zhang, *Nature*, 2017, **546**, 265–269.
7 B. Huang, G. Clark, E. Navarro-Moratalla, D. R. Klein, R. Cheng, K. L. Seyler, D. Zhong, E. Schmidgall, M. A. McGuire, D. H. Cobden, W. Yao, D. Xiao, P. Jarillo-Herrero and X. Xu, *Nature*, 2017, **546**, 270–273.
8 M. Bonilla, S. Kolekar, Y. Ma, H. C. Diaz, V. Kalappattil, R. Das, T. Eggers, H. R. Gutierrez, M.-H. Phan and M. Batzill, *Nat. Nanotechnol.*, 2018, **13**, 289–293.
9 S. Y. Kim, T. Y. Kim, L. J. Sandilands, S. Sinn, M.-C. Lee, J. Son, S. Lee, K.-Y. Choi, W. Kim, B.-G. Park, C. Jeon, H.-D. Kim, C.-H. Park, J.-G. Park, S. J. Moon and T. W. Noh, *Phys. Rev. Lett.*, 2018, **120**, 136402.
10 Z. Fei, B. Huang, P. Malinowski, W. Wang, T. Song, J. Sanchez, W. Yao, D. Xiao, X. Zhu, A. F. May, W. Wu, D. H. Cobden, J.-H. Chu and X. Xu, *Nat. Mater.*, 2018, **17**, 778–782.
11 D. Zhong, K. L. Seyler, X. Linpeng, R. Cheng, N. Sivadas, B. Huang, E. Schmidgall, T. Taniguchi, K. Watanabe, M. A. McGuire, W. Yao, D. Xiao, K.-M. C. Fu and X. Xu, *Sci. Adv.*, 2017, **3**, e1603113.
12 K. L. Seyler, D. Zhong, D. R. Klein, S. Gao, X. Zhang, B. Huang, E. Navarro-Moratalla, L. Yang, D. H. Cobden, M. A. McGuire, W. Yao, D. Xiao, P. Jarillo-Herrero and X. Xu, *Nat. Phys.*, 2018, **14**, 277–281.

13 S. Jiang, J. Shan and K. F. Mak, *Nat. Mater.*, 2018, **17**, 406–410.
14 S. Jiang, L. Li, Z. Wang, K. F. Mak and J. Shan, *Nat. Nanotechnol.*, 2018, **13**, 549–553.
15 B. Huang, G. Clark, D. R. Klein, D. MacNeill, E. Navarro-Moratalla, K. L. Seyler, N. Wilson, M. A. McGuire, D. H. Cobden, D. Xiao, W. Yao, P. Jarillo-Herrero and X. Xu, *Nat. Nanotechnol.*, 2018, **13**, 544–548.
16 Z. Wang, T. Zhang, M. Ding, B. Dong, Y. Li, M. Chen, X. Li, J. Huang, H. Wang, X. Zhao, Y. Li, D. Li, C. Jia, L. Sun, H. Guo, Y. Ye, D. Sun, Y. Chen, T. Yang, J. Zhang, S. Ono, Z. Han and Z. Zhang, *Nat. Nanotechnol.*, 2018, **13**, 554–559.
17 T. Song, X. Cai, M. W.-Y. Tu, X. Zhang, B. Huang, N. P. Wilson, K. L. Seyler, L. Zhu, T. Taniguchi, K. Watanabe, M. A. McGuire, D. H. Cobden, D. Xiao, W. Yao and X. Xu, *Science*, 2018, **360**, 1214–1218.
18 D. R. Klein, D. MacNeill, J. L. Lado, D. Soriano, E. Navarro-Moratalla, K. Watanabe, T. Taniguchi, S. Manni, P. Canfield, J. Fernández-Rossier and P. Jarillo-Herrero, *Science*, 2018, eaar3617.
19 Z. Wang, I. Gutiérrez-Lezama, N. Ubrig, M. Kroner, M. Gibertini, T. Taniguchi, K. Watanabe, A. Imamoğlu, E. Giannini and A. F. Morpurgo, *Nat. Commun.*, 2018, **9**, 2516.
20 H. H. Kim, B. Yang, T. Patel, F. Sfigakis, C. Li, S. Tian, H. Lei and A. W. Tsen, *Nano Lett.*, 2018, **18**, 4885–4890.
21 C. Cardoso, D. Soriano, N. A. García-Martínez and J. Fernández-Rossier, *Phys. Rev. Lett.*, 2018, **121**, 067701.
22 Y. Zhang, H. Lu, X. Zhu, S. Tan, W. Feng, Q. Liu, W. Zhang, Q. Chen, Y. Liu, X. Luo, D. Xie, L. Luo, Z. Zhang and X. Lai, *Sci. Adv.*, 2018, **4**, eaao6791.
23 Y. Deng, Y. Yu, Y. Song, J. Zhang, N. Z. Wang, Z. Sun, Y. Yi, Y. Z. Wu, S. Wu, J. Zhu, J. Wang, X. H. Chen and Y. Zhang, *Nature*, 2018, **563**, 94.
24 Z. Wang, D. Sapkota, T. Taniguchi, K. Watanabe, D. Mandrus and A. F. Morpurgo, *Nano Lett.*, 2018, **18**, 4303–4308.
25 Q. Li, M. Yang, C. Gong, R. V. Chopdekar, A. T. N'Diaye, J. Turner, G. Chen, A. Scholl, P. Shafer, E. Arenholz, A. K. Schmid, S. Wang, K. Liu, N. Gao, A. S. Admasu, S.-W. Cheong, C. Hwang, J. Li, F. Wang, X. Zhang and Z. Qiu, *Nano Lett.*, 2018, **18**, 5974–5980.
26 K. Kim, J. Seo, E. Lee, K.-T. Ko, B. S. Kim, B. G. Jang, J. M. Ok, J. Lee, Y. J. Jo, W. Kang, J. H. Shim, C. Kim, H. W. Yeom, B. I. Min, B.-J. Yang and J. S. Kim, *Nat. Mater.*, 2018, **17**, 794–799.
27 C. Tan, J. Lee, S.-G. Jung, T. Park, S. Albarakati, J. Partridge, M. R. Field, D. G. McCulloch, L. Wang and C. Lee, *Nat. Commun.*, 2018, **9**, 1554.
28 T. Song, M. W.-Y. Tu, C. Carnahan, X. Cai, T. Taniguchi, K. Watanabe, M. A. McGuire, D. H. Cobden, D. Xiao, W. Yao and X. Xu, *Nano Lett.*, 2019, **19**, 915–920.
29 N. D. Mermin and H. Wagner, *Phys. Rev. Lett.*, 1966, **17**, 1133–1136.
30 H.-J. Deiseroth, K. Aleksandrov, C. Reiner, L. Kienle and R. K. Kremer, *Eur. J. Inorg. Chem.*, 2006, **2006**, 1561–1567.
31 B. Chen, J. Yang, H. Wang, M. Imai, H. Ohta, C. Michioka, K. Yoshimura and M. Fang, *J. Phys. Soc. Jpn.*, 2013, **82**, 124711.
32 V. Y. Verchenko, A. A. Tsirlin, A. V. Sobolev, I. A. Presniakov and A. V. Shevelkov, *Inorg. Chem.*, 2015, **54**, 8598–8607.
33 A. F. May, S. Calder, C. Cantoni, H. Cao and M. A. McGuire, *Phys. Rev. B: Condens. Matter Mater. Phys.*, 2016, **93**, 014411.
34 J. Yi, H. Zhuang, Q. Zou, Z. Wu, G. Cao, S. Tang, S. A. Calder, P. R. C. Kent, D. Mandrus and Z. Gai, *2D Mater.*, 2017, **4**, 011005.
35 S. Grimme, *J. Comput. Chem.*, 2006, **27**, 1787–1799.
36 S. Grimme, J. Antony, S. Ehrlich and H. Krieg, *J. Chem. Phys.*, 2010, **132**, 154104.
37 M. Dion, H. Rydberg, E. Schröder, D. C. Langreth and B. I. Lundqvist, *Phys. Rev. Lett.*, 2004, **92**, 246401.
38 G. Román-Pérez and J. M. Soler, *Phys. Rev. Lett.*, 2009, **103**, 096102.
39 S. Grimme, S. Ehrlich and L. Goerigk, *J. Comput. Chem.*, 2011, **32**, 1456–1465.
40 J. Klimeš, D. R. Bowler and A. Michaelides, *Phys. Rev. B: Condens. Matter Mater. Phys.*, 2011, **83**, 195131.
41 D. M. Ceperley and B. J. Alder, *Phys. Rev. Lett.*, 1980, **45**, 566–569.
42 J. P. Perdew and A. Zunger, *Phys. Rev. B: Condens. Matter Mater. Phys.*, 1981, **23**, 5048–5079.
43 J. P. Perdew, K. Burke and M. Ernzerhof, *Phys. Rev. Lett.*, 1996, **77**, 3865–3868.
44 J. P. Perdew, A. Ruzsinszky, G. I. Csonka, O. A. Vydrov, G. E. Scuseria, L. A. Constantin, X. Zhou and K. Burke, *Phys. Rev. Lett.*, 2008, **100**, 136406.
45 A. Tkatchenko and M. Scheffler, *Phys. Rev. Lett.*, 2009, **102**, 073005.
46 S. N. Steinmann and C. Corminboeuf, *J. Chem. Theory Comput.*, 2011, **7**, 3567–3577.
47 S. N. Steinmann and C. Corminboeuf, *J. Chem. Phys.*, 2011, **134**, 044117.
48 K. Lee, É. D. Murray, L. Kong, B. I. Lundqvist and D. C. Langreth, *Phys. Rev. B: Condens. Matter Mater. Phys.*, 2010, **82**, 081101.
49 T. Oguchi, K. Terakura and A. R. Williams, *Phys. Rev. B: Condens. Matter Mater. Phys.*, 1983, **28**, 6443–6452.
50 A. I. Liechtenstein, M. I. Katsnelson, V. P. Antropov and V. A. Gubanov, *J. Magn. Magn. Mater.*, 1987, **67**, 65–74.
51 M. J. Han, T. Ozaki and J. Yu, *Phys. Rev. B: Condens. Matter Mater. Phys.*, 2004, **70**, 184421.
52 H. Yoon, T. J. Kim, J.-H. Sim, S. W. Jang, T. Ozaki and M. J. Han, *Phys. Rev. B: Condens. Matter Mater. Phys.*, 2018, **97**, 125132.
53 J.-X. Zhu, M. Janoschek, D. S. Chaves, J. C. Cezar, T. Durakiewicz, F. Ronning, Y. Sassa, M. Mansson, B. L. Scott, N. Wakeham, E. D. Bauer and J. D. Thompson, *Phys. Rev. B: Condens. Matter Mater. Phys.*, 2016, **93**, 144404.
54 Y. Liu, V. N. Ivanovski and C. Petrovic, *Phys. Rev. B: Condens. Matter Mater. Phys.*, 2017, **96**, 144429.
55 Y. Liu, E. Stavitski, K. Attenkofer and C. Petrovic, *Phys. Rev. B: Condens. Matter Mater. Phys.*, 2018, **97**, 165415.

56 Here our number counting is simply based on the ionic picture. In the metallic picture, all valence electrons can contribute and therefore the number would differ. The reality is likely somewhere in between. The differences between the two data sets (i.e., green and magenta) reflect this difference.

57 Among the samples reported in ref. 33, range of defects for a few cases is outside our theoretical range of the FM ground state. However, it should be regarded as the exceptional case rather than general. Considering that all the other experimental refinement data (see, e.g., ref. 30, 32, 53, 54, and 55) fall in our range, our estimated range of the FM ground state is in good agreement with experiments. It should also be noted that the theoretical charge counting cannot be identical with experimental one.

58 J. Kim, S. S. Baik, S. H. Ryu, Y. Sohn, S. Park, B.-G. Park, J. Denlinger, Y. Yi, H. J. Choi and K. S. Kim, *Science*, 2015, **349**, 723–726.

59 S. S. Baik, K. S. Kim, Y. Yi and H. J. Choi, *Nano Lett.*, 2015, **15**, 7788–7793.

60 G. Kresse and D. Joubert, *Phys. Rev. B: Condens. Matter Mater. Phys.*, 1999, **59**, 1758–1775.

61 http://www.openmx-square.org.

62 T. Ozaki, *Phys. Rev. B: Condens. Matter Mater. Phys.*, 2003, **67**, 155108.

63 K. Haule, C.-H. Yee and K. Kim, *Phys. Rev. B: Condens. Matter Mater. Phys.*, 2010, **81**, 195107.